AIP | Physics of Fluids

Experimental study of drop spreading on textured superhydrophilic surfaces

Seong Jin Kim, Jungchul Kim, Myoung-Woon Moon, Kwang-Ryeol Lee, and Ho-Young Kim

Citation: Phys. Fluids **25**, 092110 (2013); doi: 10.1063/1.4821985
View online: http://dx.doi.org/10.1063/1.4821985
View Table of Contents: http://pof.aip.org/resource/1/PHFLE6/v25/i9
Published by the AIP Publishing LLC.

PHYSICS OF FLUIDS **25**, 092110 (2013)

Experimental study of drop spreading on textured superhydrophilic surfaces

Seong Jin Kim,[1] Jungchul Kim,[2] Myoung-Woon Moon,[1] Kwang-Ryeol Lee,[1] and Ho-Young Kim[2,a)]
[1]*Institute for Multi-disciplinary Convergence of Matter, Korea Institute of Science and Technology, Seoul 136-791, South Korea*
[2]*Department of Mechanical and Aerospace Engineering, Seoul National University, Seoul 151-744, South Korea*

(Received 16 October 2012; accepted 5 September 2013; published online 27 September 2013)

The spreading dynamics of a drop deposited on a superhydrophilic micropillar array are qualitatively different from those on a smooth surface in that a thin fringe layer rapidly wicks into microstructures while the bulk collapses in the center. Here we experimentally measure the temporal evolution of the shapes of water and silicone oil drops on the superhydrophilic surfaces, and find various power laws that describe the spreading dynamics. The bulk radius increases initially but shrinks in the late stages for drainage of its volume by wicking. The fringe film tends to grow diffusively for the entire timespan of spreading with the effective diffusivity being a function of surface tension, pillar height, viscosity, and surface roughness. The entire footprint is shown to grow like $t^{1/4}$, t being time, for the entire time range, which allows us to estimate the time for complete drop spreading. © *2013 AIP Publishing LLC*. [http://dx.doi.org/10.1063/1.4821985]

I. INTRODUCTION

When a solid surface is microtextured, its intrinsic wettability is magnified so that a hydrophilic surface becomes superhydrophilic and a hydrophobic surface superhydrophobic. While dynamic behavior of liquid drops on superhydrophobic surfaces has been studied extensively,[1–4] the dynamics of drops deposited on superhydrophilic surfaces have drawn limited scientific interest to date.[5,6] A small viscous drop on highly wettable smooth solid surfaces (e.g., a silicon oxide surface treated by oxygen plasma) maintains a spherical-cap shape at each instant during spreading[7] as shown in Fig. 1(a). On the other hand, when a drop is brought into contact with a rough hydrophilic, or superhydrophilic, surface, the upper part of the drop collapses while the fringe layer wicks into the surface texture as shown in Fig. 1(b). The final shape is thus a thin film with its thickness and area defined by the geometric structures of the rough surface. McHale *et al*.[8] observed the deviation of drop shape from a spherical cap due to drainage of bulk into a film filling the pillar gaps, but no account was given of the dynamics of each portion of the drop. The very early stage dynamics of this superwetting process were analyzed by Kim *et al*.,[6] in which the radial extent of the fringe film was small compared to the bottom radius of the bulk.

The spreading of liquid drops on highly wettable rough solid surfaces is frequently found in everyday lives, including an ink drop on paper and a rain drop impacting on fabric or soil. In HVAC (heating, ventilation, and air-conditioning) industry, the efficiency of heat and mass transfer in evaporative coolers, absorption refrigeration systems, and condensers is a sensitive function of the spreading characteristics of drops on the device surfaces. A recently suggested scheme to fabricate inexpensive microfluidic devices utilizes spreading of a biofluid on hydrophilicized paper.[9] Animals living in arid environments, such as desert lizards, *Moloch horridus* of Australia,[10] and desert horned

a)Author to whom correspondence should be addressed. Electronic mail: hyk@snu.ac.kr

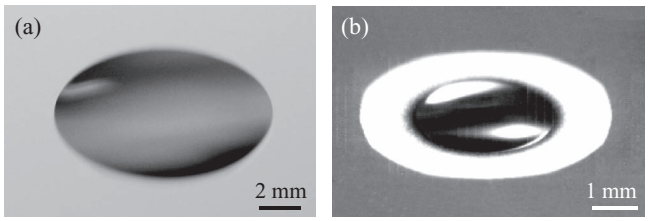

FIG. 1. (a) A silicone oil drop with an initial radius 0.62 mm spreading on a smooth silicon oxide surface treated by oxygen plasma. (b) A silicone oil drop with an initial radius 0.71 mm spreading and wicking on a superhydrophilic array of square pillars of 16, 15, and 20 μm in height, width, and spacing, respectively.

lizards, *Phrynosoma platyrhinos* of North America,[11] rely on the spreading and transport of water drops collected on their rough body surface for water ingestion.[12,13]

The spreading dynamics of a liquid drop are in general governed by the interaction of the collapsing bulk and the wicking fringe film. The bulk acts as both a reservoir to supply the fringe film with liquid and a region of high pressure due to its curvature. The fringe propagates radially outward through the gaps of micropillars by capillary action but also appears to extend inward in the late stages due to shrinkage of the bulk. These constitute a rich, yet unexplored problem involving the spreading (and shrinking) of a bulk drop and wicking of liquid film emanating from the source of a variable volume (bulk). Here we present quantitative measurement results of the temporal evolution of shape of drops on superhydrophilic surfaces, and then discuss the power-law behavior observed in each portion of the drop.

II. EXPERIMENTAL

As a superhydrophilic surface, we use a micropillar array fabricated on a silicon wafer using the deep reactive ion etching process. The surface is coated with the Si-incorporated diamond-like carbon film and treated by oxygen plasma. The result is a superhydrophilic surface with controlled surface texture. For detailed process conditions, see Yi *et al.*[14] We vary the height (h), width (w), and spacing (d) of the square pillars as shown in Fig. 2(a), so that $\{h, w, d\} \in [10\ 20]$ μm. Drop liquids used in the experiments are deionized water with density $\rho = 1000$ kg/m^3, viscosity $\mu = 1.3 \times 10^{-3}$ Pa s, and surface tension $\sigma = 0.074$ N/m, and silicone oil with $\rho = 980$ kg/m^3, $\mu = 0.091$ Pa s, and $\sigma = 0.021$ N/m. The characteristic velocity $U_c = \sigma/\mu$, which typically appears in capillary phenomena in viscous regimes,[15] is 57 and 0.23 m/s for water and silicone oil, respectively. The equilibrium contact angles of water and silicone oil with the flat surfaces treated in the identical manner to the process above are measured to be $2.6^\circ \pm 0.2^\circ$ and $2.0^\circ \pm 0.6^\circ$, respectively, using sessile drops of 1 μl volume. Drops of various radii, $a \in [0.3\ 0.9]$ mm, are deposited on the horizontally situated micropillar arrays using a micropipette. The drops arrive at the substrates with a speed less than 2 mm/s for all the cases. Since the impact Weber number, defined as $We = \rho U^2 a/\sigma$ with U being the impact velocity, is at most 10^{-4}, the effect of inertia compared to surface tension is negligible. A high-speed camera system records the liquid motion at a frame rate up to 100 s^{-1}.

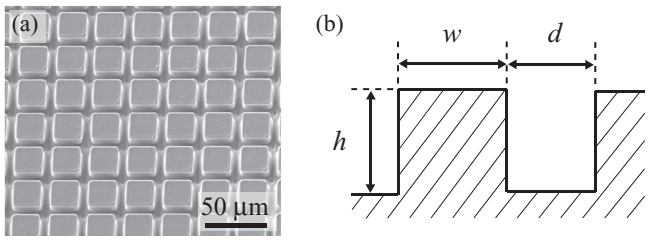

FIG. 2. (a) A scanning electron microscopy image of the square micropillar array. (b) Dimensions of the square micropillar array.

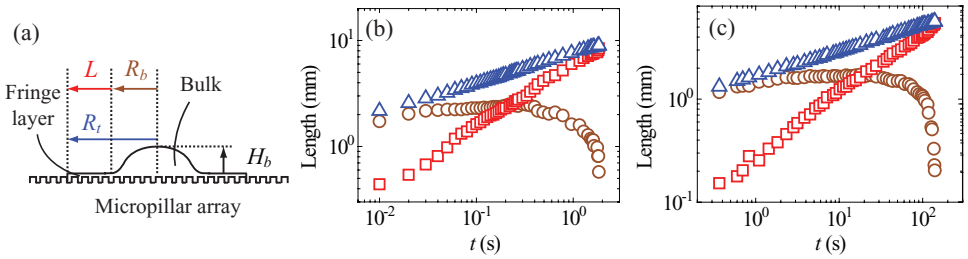

FIG. 3. (a) Schematic of a liquid drop deposited on a superhydrophilic micropillar array. The experimental measurement results of the bulk radius, R_b (circle), the entire footprint, R_t (triangle), and the radial extent of the fringe film, L (square), versus time for drops of (b) water and (c) silicone oil. $[a, h, w, d] = [760, 10, 15, 10]$ μm for (b) and [640, 13, 10, 10] μm for (c).

III. RESULTS AND DISCUSSION

Since the drop consists of a central bulk and a fringe layer during spreading as illustrated in Fig. 3(a), its interaction with the solid surface can be described with the bottom radius, R_b, of the bulk and the radius of entire footprint, R_t. The radial extent of the fringe film, i.e., the distance between the edges of the bulk and the entire footprint, is $L = R_t - R_b$. Figures 3(b) and 3(c) show the experimentally measured representative temporal evolution of R_b, L, and R_t of water and silicone oil drops, respectively. In the very early stages, all of them increase with time, t, indicating that the bulk increases in its bottom radius while the fringe film propagates ahead of it. The bulk radius subsequently plateaus and decreases as a significant amount of liquid in the bulk is drained into the film. Its decrease is accelerated toward the end of the spreading process when the bulk vanishes. The water drop tends to spread much faster than the silicone oil drop because of higher surface tension and lower viscosity of water. It is interesting to see that the log-log plots clearly reveal the power-law behavior of R_b in early stages and L and R_t in the entire time range.

We use dimensional analysis to understand the measured behavior of the drops. The scaled dimensions of the drop, R_b/a, R_t/a, and L/a, must be a function of some dimensionless parameters. In addition to the dimensionless time, tU_c/a, there are three other dimensionless length scales in the problem: the scaled pillar height, h/a, the roughness, r, defined as the ratio of the actual surface area to the projected area, and the ratio of the basal area not covered by pillars to the entire projected area, f. Simple geometric considerations lead to $r = 1 + 4wh/(w + d)^2$ and $f = 1 - w^2/(w + d)^2$. Thus, we find that X/a is a function of tU_c/a, h/a, r, and f, where X can be any instantaneous dimension of the drop.

A. Collapsing dynamics of bulk

In Fig. 4, we plot the dimensionless bulk radius, R_b/a, versus the dimensionless time tU_c/a for different scaled parameters of surface microtexture, h/a, r, and f. In the early stages, all the data of R_b/a collapse onto a single curve, implying that they depend only on tU_c/a regardless of dimensions of surface microtextures. The corresponding physics were elucidated by Kim *et al.*[6] which balanced the driving force for the bulk spreading due to capillarity, $F_{d,b} \sim R_b\sigma(1 - \cos\theta) \sim R_b\sigma\theta^2$, with the viscous resistant force $F_{r,b} \sim \mu H_b R_b(\dot{R}_b/R_b)$, where θ is the advancing contact angle ($\sim H_b/R_b$). Due to the high mobility of the underlying liquid film that wicks into the gaps of micropillars,[16,17] the spreading dynamics of bulk differs considerably from what is expected on a smooth dry solid, Tanner's law.[18] In the early stages when $H_b \sim a^3/R_b^2$, we get $R_b/a \sim (tU_c/a)^{1/4}$. In Appendix, we discuss the role of the mobility of the underlying liquid film in the spreading behavior of the bulk. We note that a power law different from Tanner's law for the spreading radius of a liquid drop on a thick, pre-deposited liquid film was reported in Ref. 17, which showed that the power n approaches 1/4 in $R_b \sim t^n$ as the film thickness increases, a result consistent with our measurements.

As time elapses, the foregoing analysis fails due to the following reasons. First, the loss of volume in the bulk due to drainage into the fringe film is no longer negligible, and thus H_b does

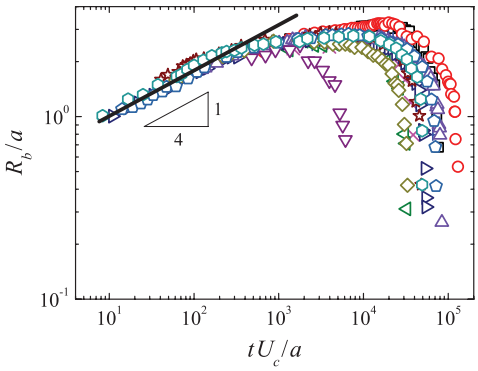

water	h (μm)	w (μm)	d (μm)	a (mm)	h/a (%)	r	f
□	10	10	15	0.75	1.3	1.6	0.84
○	10	15	10	0.76	1.3	2.0	0.64
+	13	15	15	0.86	1.6	1.7	0.75
×	14	15	20	0.82	1.7	1.7	0.82
◁	16	10	10	0.77	2.1	2.6	0.75

oil	h (μm)	w (μm)	d (μm)	a (mm)	h/a (%)	r	f
▷	13	10	10	0.64	2.0	2.3	0.75
⬡	13	10	15	0.82	1.6	1.8	0.84
⬠	13	10	20	0.90	1.4	1.6	0.89
△	13	15	10	0.68	1.9	2.2	0.64
▽	14	15	15	0.29	4.8	1.9	0.75
☆	16	15	10	0.83	1.9	2.5	0.64
◇	20	15	10	0.78	2.6	2.9	0.64

FIG. 4. Temporal evolution of a dimensionless bulk radius. In the early stages ($tU_c/a < 300$), the arithmetic average of the slopes of the best-fitting lines of each experimental condition is 0.23 with the standard deviation of 0.093.

not follow $\sim a^3/R_b^2$. Rather, H_b is coupled to L as well as a and R_b because the instantaneous bulk volume $\sim R_b^2 H_b$ is given by the original drop volume $\frac{4}{3}\pi a^3$ minus the film volume $\pi(R_b + L)^2$. As will get clear below, L is a sensitive function of surface microtextures. Second, the bulk radius shrinks while the uncompensated Young force,[19] $\sim R_b\sigma(1 - \cos\theta)$, is continually at work. This is one of the rare examples where the contact line with the dynamic contact angle larger than the equilibrium value (near zero) recedes, posing an intriguing problem worth further exploration. Shrinkage of a drop base radius, a similar phenomenon to the one observed here, was reported for a drop that evaporates as it spreads on a completely wettable surface,[20] where the base radius R was shown to follow the power law $R \propto (t_0 - t)^y$ with t_0 being the time when the drop totally disappears and y the empirical power close to 0.5. This system is different from ours in that the volume reduction is through the mass outflux over the entire liquid-gas interface while in the current work, the bulk volume is sucked into the gaps of micropillars only at the bulk-fringe boundary.

Since the decrease of R_b in the late stages is caused by the drainage of liquid into the fringe film, it is natural to relate the time when R_b starts to decrease, τ_m, to a parameter β signifying the ratio of the initial drop volume to drainage volume. In Sec. III B, we show that a function of the roughness, $\phi = (r - 1)/r$, and the film thickness h determine the film propagation rate. Taking $\beta = [a/(\phi h)]^2$, which will be derived below, we see that a dimensionless time for maximum bulk radius, $\tau_m U_c/a$, tends to collapse onto a single curve when plotted against β (Fig. 5). $\tau_m U_c/a$ tends to linearly increase with β, whose slope (0.55) will be further discussed in Sec. III C. In physical terms, as the roughness and scaled pillar height increase (leading to the increase of wicking rate and

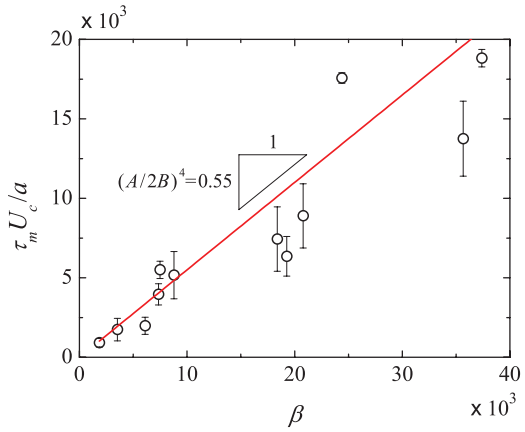

FIG. 5. Dependence of the dimensionless time when the bulk radius starts to decrease upon β.

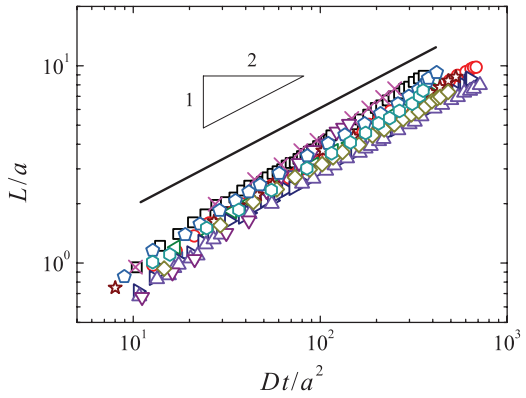

FIG. 6. Temporal evolution of L/a versus a scaled time, Dt/a^2.

volume of fringe film, and thus smaller β), R_b tends to start to decrease earlier in the scaled time, yielding smaller $\tau_m U_c/a$.

B. Extension of fringe film

Now we turn to the spreading of a fringe film that goes through hemi-wicking, i.e., two-dimensional wicking on a textured surface.[21] Before we address the fringe film occurring in our drop deposition process, we first consider a liquid film that propagates from an infinite, stationary source. The propagation of such a film is known to exhibit the diffusive dynamics, allowing us to write $l \sim \sqrt{Dt}$, where l is the propagation distance from the source and D is the effective diffusivity. For a straight front of liquid rising from a bath along the vertically situated superhydrophilic wall, the driving capillary and resisting viscous forces per unit width are scaled as $F'_{d,f} \sim (r-1)\sigma$ and $F'_{r,f} \sim \mu r \dot{l} l/h$, respectively.[6,22] Here subscripts d, r, and f denote driving, resisting, and film, respectively. Then we get $D \sim \phi\sigma h/\mu$, where $\phi = (r-1)/r$. A similar model applies to an axisymmetric propagation of a film from a stationary point source like a pen[22] with $F_{d,f} \sim (r-1)\sigma R_s$ and $F_{r,f} \sim \mu \dot{R}_s R_s^2 r/h$, which yields the radius of a circular blot, $R_s \sim \sqrt{Dt}$.

The temporal evolution of the radial extent of fringe film, L, during the drop spreading considered here needs to be treated with caution. The bottom radius of the liquid reservoir, or the bulk, grows and subsequently shrinks while the outer edge propagates. Thus, L must be measured between the edges of bulk and entire footprint, both of which move with time: $L(t) = R_t(t) - R_b(t)$. Motivated by the fact that the dimensionless timescale obtained from the diffusive dynamics analysis, Dt/a^2, is expressed as the product of the following dimensionless parameters, ϕ, h/a, and tU_c/a, we plot L/a versus $Dt/a^2 = \phi(h/a)tU_c/a$ in Fig. 6 to find that all the data tend to collapse onto a straight line. The arithmetic average of the slopes of the best-fitting lines for each experimental condition is 0.60 with the standard deviation of 0.078. This is in reasonable agreement with the diffusive behavior, $L \sim t^{1/2}$, as previously observed by Courbin *et al.*[5] for the similar system. The diffusive dynamics can be explained as the following: balancing $F_{d,f} \sim R_t(r-1)\sigma$ with $F_{r,f} \sim \mu r U(R_t^2 - R_b^2)/h$ while taking $U \sim \dot{L}$ gives $L\dot{L} \sim (\phi\sigma h/\mu)(1 + R_b/R_t)^{-1}$. Because $(R_b/R_t) \ll 1$ when $L/a > 1$, we get $L \sim (Dt)^{1/2}$. The empirical relation between L/a and Dt/a^2 can be established as the following via the least squares method:

$$\frac{L}{a} = 0.36\sqrt{\frac{Dt}{a^2}}. \tag{1}$$

C. Spreading of entire footprint

The radius of entire footprint, R_t, is a sum of the bulk radius and fringe extension: $R_t = R_b + L$. In the early stages when $R_b \gg L$, R_t must follow the behavior of R_b, and thus it is natural to write

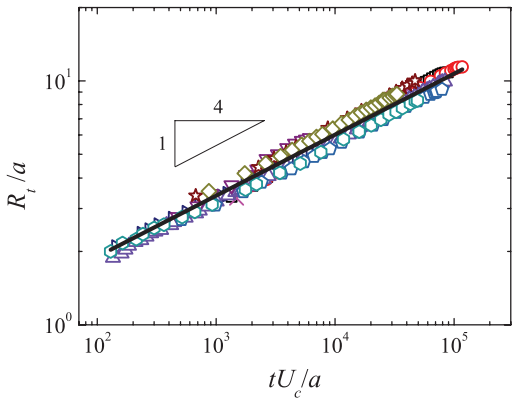

FIG. 7. The scaled radius of the entire footprint, R_t/a, versus a scaled time, tU_c/a. The arithmetic average of the slopes of the best-fitting lines of each experimental condition is 0.28 with the standard deviation of 0.018.

$R_t/a \sim (tU_c/a)^{1/4}$.[6] Surprisingly, when plotting R_t/a versus the scaled time tU_c/a as in Fig. 7, we find that all the experimental data tend to collapse onto a single straight line with a slope of 1/4 even beyond the early stages. Thus, the radius of entire footprint, which spreads like $t^{1/4}$ throughout the time, can be expressed by the following general empirical relationship using the dimensionless parameters:

$$\frac{R_t}{a} = 0.62\left(\frac{tU_c}{a}\right)^{1/4}. \tag{2}$$

There are two remarkable features in this relationship. First, the spreading of entire footprint is independent of the detailed surface structures, but only depends on the liquid properties (σ and μ) and the initial drop radius. That is, R_t/a depends only on tU_c/a, not on the other independent dimensionless parameters such as h/a, r, and f. Second, while the fringe film that propagates like $t^{1/2}$ as a function of ϕ dominates over R_b in the late stages, such an effect is not pronounced in the spreading rate of R_t. As mentioned above, the temporal evolutions of R_b and L are interrelated because the mass of the initial drop should be conserved. The increase in the fringe area causes the deceleration of the bulk spreading and eventually the shrinkage of the bulk. The different power laws of L and R_t are rationally explained by supposing that the temporal evolution of R_b absorbs the effects of L.

Using the empirical relation (2), we can further understand the behavior of R_b that undergoes growth and subsequent decrease during the course of drop spreading. Since $R_b = R_t - L$, we

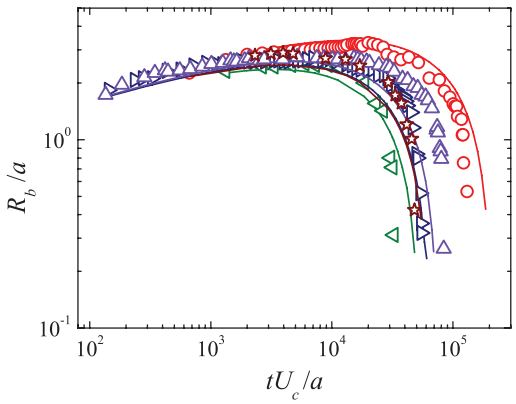

FIG. 8. The scaled bulk radius, R_b/a, plotted according to Eq. (3). The lines plot Eq. (3) for each condition.

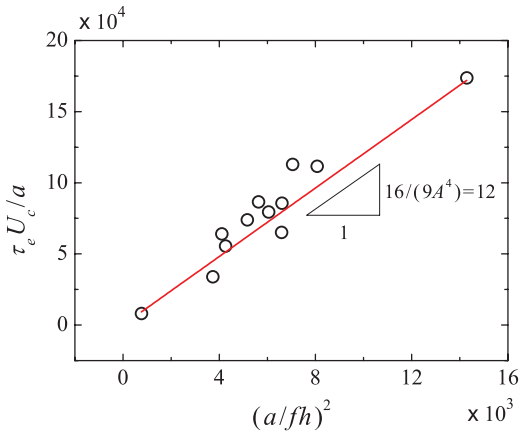

FIG. 9. The dimensionless time for complete spreading versus $[a/(fh)]^2$. The line plots Eq. (5).

empirically get

$$\frac{R_b}{a} = A\left(\frac{tU_c}{a}\right)^{1/4} - B\frac{\sqrt{Dt}}{a}, \tag{3}$$

where $A = 0.62$ and $B = 0.36$. It follows that when $t \ll (A/B)^4 a^3\mu/(\phi^2\sigma h^2)$, the first term in the left-hand side of Eq. (3) dominates, and thus we recover $R_b/a \sim (tU_c/a)^{1/4}$. We compare Eq. (3) with the experimental data in Fig. 8, to find reasonable agreement between them. By differentiating Eq. (3) with t, we find the time, τ_m, at which R_b reaches the maximum:

$$\frac{\tau_m U_c}{a} = \left(\frac{A}{2B}\right)^4 \frac{1}{\phi^2}\left(\frac{a}{h}\right)^2. \tag{4}$$

As mentioned earlier, R_b starts to decrease earlier with the increase of ϕ and h/a because of promoted drainage of liquid into fringe, whose tendency has been experimentally observed in Fig. 5. We note that the coefficient of proportionality, $[A/(2B)]^4 = 0.55$ in Eq. (4), agrees well with the slope found in Fig. 5.

The simple dependency of R_t/a on the dimensionless time tU_c/a also allows us to predict the time taken for a drop to complete its spreading. Balancing the original drop volume, $\frac{4}{3}\pi a^3$, with the volume of liquid film that fills the gaps of the pillars, $\pi R_t^2(t)hf$, gives the time for complete spreading, τ_e:

$$\frac{\tau_e U_c}{a} = \frac{16}{9A^4}\frac{1}{f^2}\left(\frac{a}{h}\right)^2, \tag{5}$$

where the proportionality constant $16/(9A^4) = 12$. We see reasonable agreement between Eq. (5) and the experimental measurements in Fig. 9. The spreading takes shorter on the substrates with sparse (high f) but tall pillars (high h/a), while it takes longer on the substrates with short pillars of a high areal density.

IV. CONCLUSIONS

We have presented the experimental measurement results of the temporal evolution of drop shapes on superhydrophilic micropillar arrays, and found various power laws between dimensionless parameters describing the spreading dynamics. Beyond the early stages of spreading that were covered previously,[6] we have measured and analyzed the dynamics of the bulk, fringe film, and entire footprint for the whole timespan of spreading. The bulk radius increases initially but decreases in the late stages for drainage of its volume into the microstructure—such decrease is hastened as the roughness and pillar height increase. The fringe film tends to grow diffusively with the effective

diffusivity being a function of surface tension, viscosity, pillar height, and roughness. The entire footprint is shown to simply grow like $t^{1/4}$ for the entire time range, which allows us to find empirical relationships for the temporal evolution of the bulk radius and the time for entire spreading.

The experimental data and power laws revealed in this work can be useful in numerical simulations which have begun to be conducted recently for the spreading of liquids on micropillar arrays.[23–25] Those computational works are in turn anticipated to help us to understand how the bulk height H_b evolves with time in addition to the bottom radii treated here. As experimentally found by McHale *et al.*,[8] the superwetting behavior, i.e., the fast spreading of the fringe film ahead of the collapsing bulk, can also be observed for rough surfaces which are partially wettable when flat. This was qualitatively observed in the experiments performed through this work, although a detailed analysis how the decreased hydrophilicity affects the spreading rates of each portion of drop calls for further study. Our results can be practically used to understand the spreading of liquid drops on HVAC equipments which are frequently covered with microroughness to enhance surface wettability, and to predict the biosample transport in paper-based microfluidic devices.

ACKNOWLEDGMENTS

This work was supported by KIST (Internal Project No. 2E23920), National Research Foundation (Grant Nos. 2011-0030744 and 2013034978), and Ministry of Trade, Industry and Energy (Global Excellent Technology Innovation R&D Program) of Korea, and administered via SNU-IAMD.

APPENDIX: BULK SPREADING ON A PRE-WETTED PILLAR ARRAY

To test the effects of an underlying liquid layer on the dynamic behavior of a drop, we measured the spreading of a drop on a textured superhydrophilic solid preimpregnated by the same liquid. We used a micropillar array with $h = 13$, $w = 10$, and $d = 15$ μm formed on a square silicon wafer measuring 20 mm $\times$ 20 mm. We pre-wetted the surface by depositing a silicone oil drop, which wicked into the gaps of the pillar array. By changing the size of the silicone oil drops, we changed the area of pre-wetted surface, so that one surface (surface I) was entirely wetted by silicone oil with the wet area being 400 mm^2 and the other surface (surface II) was partially wetted with the wet area being 70 mm^2. When a silicone oil drop with the radius $a = 0.82$ mm was deposited on the fully pre-wetted surface (I), no further wicking was possible because all the gaps between the pillars had already been filled with the liquid. We found that the drop deposited on surface I spreads with the bottom radius R_b following Tanner's law ($R_b \sim t^{1/10}$) as shown in Fig. 10. However, when a drop was deposited on the partially pre-wetted surface (II), R_b increased like $t^{1/4}$ in the early stages just

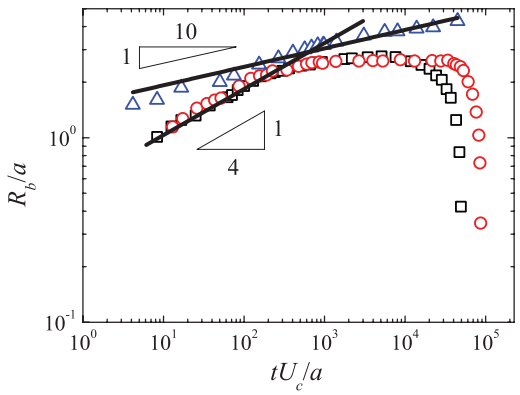

FIG. 10. Temporal evolution of the dimensionless bulk radius on dry and pre-wetted micropillar arrays with $h = 13$, $w = 10$, and $d = 15$ μm. Triangles, circles, and squares correspond to the values of R_b/a on surfaces I and II and the dry micropillar array, respectively.

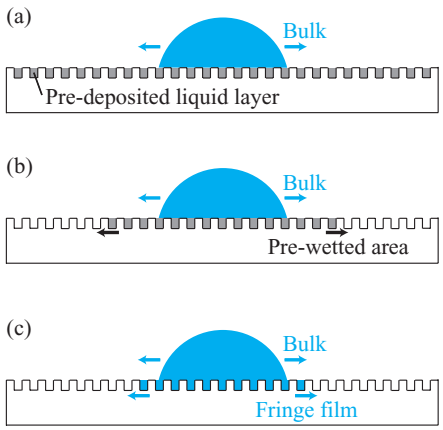

FIG. 11. Schematic illustrations of the flows associated with the bulk spreading on micropillar arrays. (a) A drop spreading on a fully pre-impregnated pillar array (surface I). (b) A drop spreading on a partially pre-impregnated pillar array (surface II). (c) A drop spreading on a dry pillar array.

as R_b of a drop deposited on the dry micropillar array, Fig. 10. These experiments reveal the crucial role of mobility of the underlying liquid layer in the spreading behavior of the drop or bulk.

As schematically illustrated in Fig. 11(a), the drop deposited on surface I spreads on a pillar array whose gaps are filled with nearly immobile liquid film, thus the velocity gradient is dominantly established across the drop height giving the viscous force as $\sim \mu R_b^2 \dot{R}_b / H_b$. Balancing this force with the driving force $\sim R_b \sigma (1 - \cos\theta) \sim R_b \sigma \theta^2$ leads to Tanner's law: $R_b/a \sim (U_c t/a)^{1/10}$. The nanoscopic precursor film that emerges ahead of the bulk of the drop does not alter this scaling law.[17] On the other hand, the drop deposited on either surface II or the dry pillar array exhibits a power law of R_b clearly different from that on surface I because of the flow within the underlying liquid layer. As can be hinted by the facts that the drop collapses into the underlying prewetted area (surface II) and that the fringe layer always precedes the bulk radius on dry pillar arrays (Fig. 11(c)), the bulk on surface II and the dry surface rides a highly mobile liquid layer that wicks into the gaps of superhydrophilic micropillar arrays. The micropillar array exerts viscous shear stresses on the liquid, but they are taken into account by the wicking of the liquid film that infiltrates the pillar gaps. Thus, the dominant velocity gradient within the bulk is given by $\dot{R}_b / R_b$, which results in the power law of $R_b \sim t^{1/4}$, consistent with experiment.

[1] D. Richard, C. Clanet, and D. Quéré, "Contact time of a bouncing drop," Nature **417**, 811 (2002).
[2] C. Clanet, C. Béguin, D. Richard, and D. Quéré, "Maximal deformation of an impacting drop," J. Fluid Mech. **517**, 199–208 (2004).
[3] Z. Wang, C. Lopez, A. Hirsa, and N. Koratkar, "Impact dynamics and rebound of water droplets on superhydrophobic carbon nanotube arrays," Appl. Phys. Lett. **91**, 023105 (2007).
[4] P. Tsai, S. Pacheco, C. Pirat, L. Lefferts, and D. Lohse, "Drop impact upon micro- and nanostructured superhydrophobic surfaces," Langmuir **25**, 12293–12298 (2009).
[5] L. Courbin, E. Denieul, E. Dressaire, M. Roper, A. Ajdari, and H. A. Stone, "Imbibition by polygonal spreading on microdecorated surfaces," Nature Mater. **6**, 661–664 (2007).
[6] S. J. Kim, M.-W. Moon, K.-R. Lee, D.-Y. Lee, Y. S. Chang, and H.-Y. Kim, "Liquid spreading on superhydrophilic micropillar arrays," J. Fluid Mech. **680**, 477–487 (2011).
[7] F. Brochard-Wyart, H. Hervet, C. Redon, and F. Rondelez, "Spreading of "heavy" droplets. I. Theory," J. Colloid Interface Sci. **142**, 518 (1991).
[8] G. McHale, N. J. Shirtcliffe, S. Aqil, C. C. Perry, and M. I. Newton, "Topography driven spreading," Phys. Rev. Lett. **93**, 036102 (2004).
[9] A. W. Martinez, S. T. Phillips, and G. M. Whitesides, "Three-dimensional microfluidic devices fabricated in layered paper and tape," Proc. Natl. Acad. Sci. U.S.A. **105**, 19606 (2008).
[10] C. Gans, R. Merlin, and W. F. C. Blumer, "The water-collecting mechanism of *Moloch horridus* re-examined," Amphib.-Reptil. **3**, 57 (1982).
[11] W. C. Sherbrooke, *Introduction to Horned Lizards of North America* (University of California Press, Berkeley, CA, 2003).
[12] P. Comanns, C. Effertz, F. Hischen, K. Staudt, W. Böhme, and W. Baumgartner, "Moisture harvesting and water transport through specialized micro-structures on the integument of lizards," Beilstein J. Nanotechnol. **2**, 204 (2011).
[13] A. Lee, M.-W. Moon, H. Lim, W.-D. Kim, and H.-Y. Kim, "Water harvest via dewing," Langmuir **28**, 10183 (2012).

[14] J. W. Yi, M.-W. Moon, S. F. Ahmed, H. Kim, T.-G. Cha, H.-Y. Kim, S.-S. Kim, and K.-R. Lee, "Long-lasting hydrophilicity on nanostructured Si-incorporated diamond-like carbon films," Langmuir **26**, 17203–17209 (2010).
[15] P.-G. de Gennes, F. Brochard-Wyart, and D. Quéré, *Capillarity and Wetting Phenomena: Drops, Bubbles, Pearls, Waves* (Springer, New York, 2004).
[16] F. Brochard-Wyart, G. Debrégeas, and P.-G. de Gennes, "Spreading of viscous droplets on a non viscous liquid," Colloid Polym. Sci. **274**, 70–72 (1996).
[17] S. L. Cormier, J. D. McGraw, T. Salez, E. Raphael, and K. Dalnoki-Veress, "Beyond Tanner's law: Crossover between spreading regimes of a viscous droplet on an identical film," Phys. Rev. Lett. **109**, 154501 (2012).
[18] L. H. Tanner, "The spreading of silicone oil drops on horizontal surfaces," J. Phys. D **12**, 1473–1484 (1979).
[19] S. Schiaffino and A. A. Sonin, "Molten drop deposition and solidification at low Weber numbers," Phys. Fluids **9**, 3172–3187 (1997).
[20] G. Guéna, C. Poulard, and A. M. Cazabat, "The leading edge of evaporating droplets," J. Colloid Interface Sci. **312**, 164–171 (2007).
[21] J. Bico, U. Thiele, and D. Quéré, "Wetting of textured surfaces," Colloids Surf. **206**, 41–46 (2002).
[22] J. Kim, M.-W. Moon, K.-R. Lee, L. Mahadevan, and H.-Y. Kim, "Hydrodynamics of writing with ink," Phys. Rev. Lett. **107**, 264501 (2011).
[23] R. Xiao, R. Enright, and E. N. Wang, "Prediction and optimization of liquid propagation in micropillar arrays," Langmuir **26**, 15070–15075 (2010).
[24] N. Srivastava, C. Din, A. Judson, N. C. MacDonald, and C. D. Meinhart, "A unified scaling model for flow through a lattice of microfabricated posts," Lab Chip **10**, 1148–1152 (2010).
[25] M. L. Blow and J. M. Yeomans, "Anisotropic imbibition of surfaces patterned with polygonal posts," Philos. Trans. R. Soc. London, Ser. A **369**, 2519–2527 (2011).